Ortho-to-para ratio of interstellar heavy water

Vastel, C.; Ceccarelli, C.; Caux, E.; Coutens, A.; Cernicharo, J.; Bottinelli, S.; Demyk, K.; Faure, A.; Wiesenfeld, L.; Scribano, Y.; Bacmann, A.; Hily-Blant, P.; Maret, S.; Walters, A.; Bergin, E.A.; Blake, G.A.; Castets, A.; Crimier, N.; Dominik, C.; Encrenaz, P.; Gérin, M.; Hennebelle, P.; Kahane, C.; Klotz, A.; Melnick, G.; Pagani, L.; Parise, B.; Schilke, P.; Wakelam, V.; Baudry, A.; Bell, T.; Benedettini, M.; Boogert, A.; Cabrit, S.; Caselli, P.; Codella, C.; Comito, C.; Falgarone, E.; Fuente, A.; Goldsmith, P.F.; Helmich, F.; Henning, T.; Herbst, E.; Jacq, T.; Kama, M.; Langer, W.; Lefloch, B.; Lis, D.; Lord, S.; Lorenzani, A.; Neufeld, D.; Nisini, B.; Pacheco, S.; Pearson, J.; Phillips, T.; Salez, M.; Saraceno, P.; Schuster, K.; Tielens, X.; van der Tak, F.; van der Wiel, M.H.D.; Viti, S.; Wyrowski, F.; Yorke, H.; Cais, P.; Krieg, J.M.; Olberg, M.; Ravera, L.

Herschel/HIFI: first science highlights

Astronomy & Astrophysics

Special feature

LETTER TO THE EDITOR

Ortho-to-para ratio of interstellar heavy water[⋆]

C. Vastel[1,2], C. Ceccarelli[3,4,5], E. Caux[1,2], A. Coutens[1,2], J. Cernicharo[6], S. Bottinelli[1,2], K. Demyk[1,2], A. Faure[3],
L. Wiesenfeld[3], Y. Scribano[7], A. Bacmann[3,4,5], P. Hily-Blant[3], S. Maret[3], A. Walters[1,2], E. A. Bergin[8], G. A. Blake[9],
A. Castets[3,4,5], N. Crimier[3,6], C. Dominik[10,11], P. Encrenaz[12], M. Gérin[12], P. Hennebelle[12], C. Kahane[3], A. Klotz[1,2],
G. Melnick[13], L. Pagani[12], B. Parise[14], P. Schilke[14,15], V. Wakelam[4,5], A. Baudry[4,5], T. Bell[9], M. Benedettini[16],
A. Boogert[17], S. Cabrit[12], P. Caselli[18], C. Codella[19], C. Comito[14], E. Falgarone[12], A. Fuente[20], P. F. Goldsmith[21],
F. Helmich[22], T. Henning[23], E. Herbst[24], T. Jacq[4,5], M. Kama[10], W. Langer[21], B. Lefloch[3], D. Lis[9], S. Lord[17],
A. Lorenzani[19], D. Neufeld[25], B. Nisini[26], S. Pacheco[3], J. Pearson[21], T. Phillips[9], M. Salez[12], P. Saraceno[16],
K. Schuster[27], X. Tielens[28], F. van der Tak[22,29], M. H. D. van der Wiel[22,29], S. Viti[30], F. Wyrowski[14], H. Yorke[21]
P. Cais[4,5], J. M. Krieg[12], M. Olberg[22,31], and L. Ravera[1,2]

(Affiliations are available on page 5 of the online edition)

ABSTRACT

Context. Despite the low elemental deuterium abundance in the Galaxy, enhanced molecular D/H ratios have been found in the environments of low-mass star-forming regions, and in particular the Class 0 protostar IRAS 16293-2422.
Aims. The CHESS (Chemical *HErschel* Surveys of Star forming regions) key program aims to study the molecular complexity of the interstellar medium. The high sensitivity and spectral resolution of the *Herschel*/HIFI instrument provide a unique opportunity to observe the fundamental $1_{1,1}-0_{0,0}$ transition of the ortho-D_2O molecule, which is inaccessible from the ground, and determine the ortho-to-para D_2O ratio.
Methods. We detected the fundamental transition of the ortho-D_2O molecule at 607.35 GHz towards IRAS 16293-2422. The line is seen in absorption with a line opacity of 0.62 ± 0.11 (1σ). From the previous ground-based observations of the fundamental $1_{1,0}-1_{0,1}$ transition of para-D_2O seen in absorption at 316.80 GHz, we estimate a line opacity of 0.26 ± 0.05 (1σ).
Results. We show that the observed absorption is caused by the cold gas in the envelope of the protostar. Using these new observations, we estimate for the first time the ortho-to-para D_2O ratio to be lower than 2.6 at a 3σ level of uncertainty, which should be compared with the thermal equilibrium value of 2:1.

Key words. astrochemistry – ISM: molecules – submillimeter: ISM – ISM: abundances – molecular processes – line: identification

1. Introduction

Among all molecules in interstellar space, water is special because of its dominant role in the cooling of warm gas and in the oxygen chemistry as well as for its role in the chemistry of the atmospheres of exoplanets and its potential connection with life. Water abundance in cold molecular gas is very low because it is frozen onto the interstellar grains and forms icy mantles around them. Although water can form theoretically by means of gaseous reactions that first form H_2O^+ and H_3O^+ (e.g. Rodgers & Charnley 2002), no observational evidence of this has yet been found. It is assumed that the major mechanism of water formation occurs on grain surfaces. One observable that helps us to discriminate between the various formation mechanisms is the abundance of single and double deuterated water relative to the normal isotopologue. Another potential discriminant is the ortho-to-para ratio (OPR), namely the ratio of water molecules with different nuclear spins. Since radiative and inelastic collisional transitions between the two ortho and para states are strongly forbidden, the OPR is set at the moment of

the water formation and is changed by nuclear spin reactions exchange later on. This can occur in either the gas phase by reactions with ions in which actual nuclei change places, or on the grain surfaces by interaction with electron spins or, perhaps, even other nuclear spins (e.g. Le Bourlot 2000; Limbach et al. 2006). Although little is known about the spin exchange in the gas phase, it is usually assumed that this is a slow process and that the OPR is likely to retain information about the moment of its formation. Emprechtinger et al. (2010); Lis et al. (2010) report determinations of the water OPR in several environments based on new *Herschel* observations. The doubly deuterated isotopologue of water, D_2O, consists of two species, ortho and para with a nuclear spin statistic weight 2:1. To date, D_2O has only been detected towards the solar-type protostar IRAS 16293-2422 (hereafter IRAS 16293), by observing the fundamental transition of the para-D_2O transition at 316.8 GHz (see our Fig. 1 and Butner et al. 2007). The observed line profile (see Fig. 2) shows a component in emission with a deep absorption at the cloud velocity ($\sim$4 km s^{-1}). The emission component has been attributed to heavy water in the hot corino of this source where the grain ices are sublimated and released into the gas phase (Ceccarelli et al. 2000; Bottinelli et al. 2004), based on the detailed analysis of several HDO lines observed in IRAS 16293
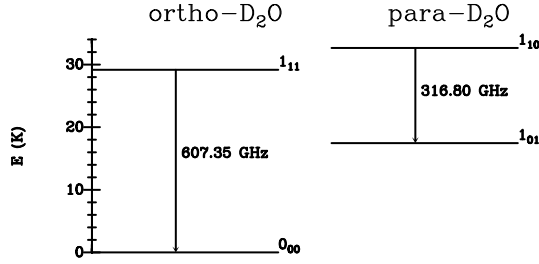
Fig. 1. Energy levels for the detected fundamental lines of D_2O.

(Parise et al. 2005). The absorption component, whose linewidth is 0.5 km s^{-1}, probably originates in the foreground gas (molecular cloud and cold envelope). Therefore, the absorption component provides a straightforward measure of the column density of para-D_2O in the cold gas surrounding IRAS 16293.

2. Observations and results

In the framework of the key program CHESS (Ceccarelli et al. 2010), we observed the solar type protostar IRAS 16293 with the HIFI instrument (de Graauw et al. 2010; Roelfsema et al. 2010) onboard the *Herschel* Space Observatory (Pillbrat et al. 2010). A full spectral coverage of band 1b between 554.5 and 636.5 GHz was performed on 2010 March 2, using the HIFI spectral scan double beam switch (DBS) mode with optimization of the continuum. The fundamental ortho-D_2O $(1_{1,1}-0_{0,0})$ transition lies in this frequency range, at 607.35 GHz (see Fig. 1). The HIFI wide band spectrometer (WBS) was used, providing a spectral resolution of 1.1 MHz ($\sim$0.55 km s^{-1} at 600 GHz) over an instantaneous bandwidth of 4×1 GHz. We note that the data are acquired at the Nyquist sampling, therefore, with 0.5 MHz steps. The targeted coordinates were $\alpha_{2000} = 16^h32^m22^s.75$, $\delta_{2000} = -24°28'34.2''$. The beam size at 610 GHz is about 35$''$, the theoretical main beam (respectively forward) efficiency is 0.72 (resp. 0.96), and the DBS reference positions were situated approximately 3$'$ east and west of the source. The data were processed using the standard HIFI pipeline up to level 2 with the ESA-supported package HIPE 3.01 (Ott et al. 2010). The 1 GHz chunks are then exported as FITS files into CLASS/GILDAS format[1] for subsequent data reduction and analysis using generic spectral survey tools developed in CLASS by our group. When present, spurs were removed in each 1 GHz scan and a low order polynomial ($\leq$2) baseline was fitted over line-free regions to correct residual bandpass effects. These polynomials were subtracted and used to determine an accurate continuum level by calculating their medians. Sideband deconvolution is computed with the minimisation algorithm of Comito & Schilke (2002) implemented into CLASS using the baseline-subtracted spectra and assuming side-band gain ratio to be unity for all tunings. Both polarisations were averaged to lower the noise in the final spectrum. The continuum values obtained are closely fitted by straight lines over the frequency range of the whole band. The single sideband continuum derived from the polynomial fit at the considered frequency was added to the spectra. Finally, the deconvolved data were analysed with CASSIS software[2]. Exact measurements of the main beam efficiency were not performed on planets at the time of our observations. However, we consider here absorption measurements, and are interested only in the relative depth of the absorption relative to the continuum level. We consequently present in the following the spectrum

[1] http://www.iram.fr/IRAMFR/GILDAS
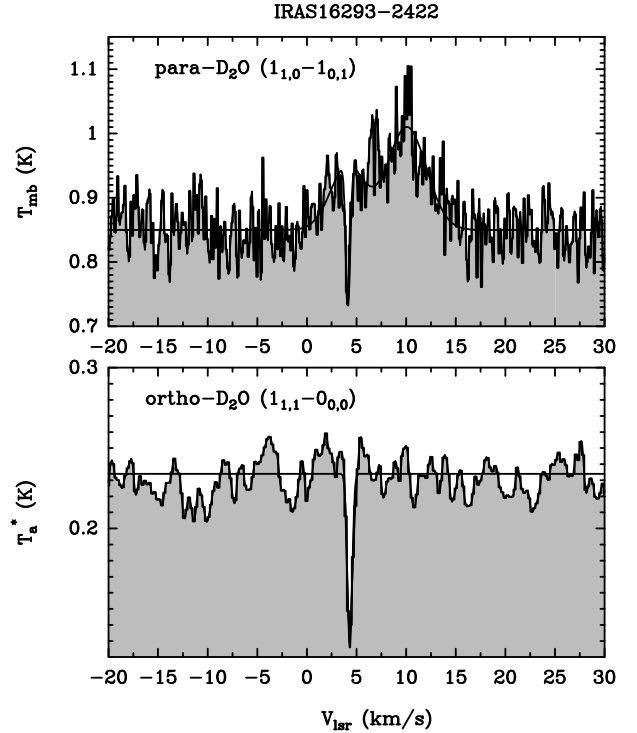[2] Developed by CESR-UPS/CNRS: http://cassis.cesr.fr

Fig. 2. Profile of the para-D_2O $(1_{1,0}-1_{0,1})$ line (histogram) observed at JCMT (*upper panel*), as well as the 3 component Gaussian fit (solid line) and ortho-D_2O $(1_{1,1}-1_{0,1})$ line observed with HIFI (*bottom panel*).

(Fig. 2) and parameters (Table 1) in T_a^* for the ortho-D_2O line. The bottom panel of Fig. 2 shows the resulting HIFI spectrum and its measured continuum level of (234 ± 19) mK (where the error includes the statistical error only). We note that the absolute accuracy of the calibration is not important when measuring absorption, since lines and continuum are affected the same way. Therefore, the main source of the uncertainty is the accuracy of the continuum. The achieved rms is about 12 mK in T_a^*, in the 0.5 MHz frequency bin. The fundamental ortho-D_2O transition at 607 349.449 MHz is clearly detected in absorption against the strong continuum, at the velocity of $\sim$4 km s^{-1}. No other lines in the image sideband are expected at this velocity. The parameters of the line, obtained using CASSIS, which takes into account the ortho and para D_2O forms separately from the Cologne Database for Molecular Spectroscopy (Müller et al. 2005; Brünken et al. 2007), are reported in Table 1. In the same table, we report also the parameters of the para-D_2O $(1_{1,0}-1_{0,1})$ fundamental line previously observed at the JCMT, published by Butner et al. (2007), at a rest frequency of 316 799.81 MHz. The data were retrieved from the JCMT archive and reduced within CLASS. We performed a 3-component Gaussian fit with CASSIS and the resulting fit is reproduced in Fig. 2 on top of the data in main beam temperatures. The para-D_2O line in emission has an intensity of 0.10 ± 0.02 K in main beam temperature, and a linewidth of 4.01 ± 0.77 km s^{-1}. The bright line at a V_{lsr} of 10.1 km s^{-1} is likely due to CH_3OD (see Butner et al. 2007) with an intensity of (0.16 ± 0.01) K and a linewidth of (4.6 ± 0.5) km s^{-1}. The parameters for the resulting fit of the para-D_2O absorption line are quoted in Table 1.

3. Determination of the D_2O OPR

Crimier et al. (2010) used the JCMT SCUBA maps of IRAS 16293 at 450 μm and 850 μm (and other data) to

Table 1. Derived parameters of the ortho and para D_2O fundamental lines.

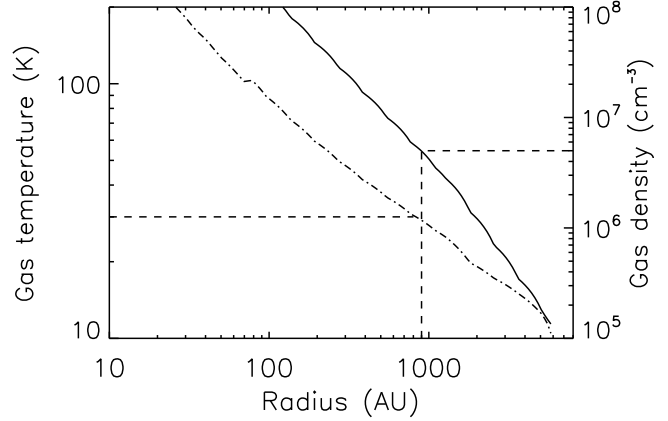| Species	Transition	Frequency GHz	Telescope	$\int T dv$ (mK km s^{-1})	$T_{abs} = T_C - T_L$ (mK)	ΔV (km s^{-1})	V_{LSR} (km s^{-1})	T_C (mK)	τ
ortho-D_2O	$1_{1,1}-0_{0,0}$	607.34945	*Herschel*	77 ± 17	108 ± 11	0.57 ± 0.09	4.33 ± 0.04	234 ± 19	0.62 ± 0.11
para-D_2O	$1_{1,0}-1_{0,1}$	316.79981	JCMT	120 ± 49	220 ± 30	0.55 ± 0.15	4.15 ± 0.04	850 ± 35	0.26 ± 0.05

Notes. Note that the parameters are in T_a^* for ortho-D_2O and T_{mb} for para-D_2O (see text).

reconstruct the structure of the IRAS 16293 envelope. From this work, one can compute the expected continuum in the HIFI beam at 607 GHz (o-D_2O line). Using their SED (Crimier et al. 2010, Fig. 1 panel d) and their Table 1, the IRAS 16293 flux is 270 ± 108 Jy at 450 μm, and the HIFI beam contains approximately 80% of the total source flux (Fig. 1, panel b). One can note that the SED steep slope ensures that the flux at 607 GHz is lower than that at 450 μm (~660 GHz) by about 30%, making the expected flux at 607 GHz be about $0.7 \times 0.8 \times (270 \pm 108)$ Jy i.e. (0.34 ± 0.14) K, using the HIFI Jy to K conversion factor (C. Kramer: Spatial response, contribution to the HIFI framework document), in perfect agreement with the observed continuum value (~0.33 K in main beam temperature). Most of the continuum, more than 70% (resp. 80%) of its peak emission at 316 GHz (resp. 607 GHz) is emitted from a region about 900 AU in radius (~15″ in diameter). The absorption of the continuum by heavy water is most likely due to the cold envelope surrounding IRAS 16293 as well as the parent cloud, much more extended than the continuum emitting region. We note that, as long as the sizes of the absorbing layer are larger than the sizes of the region emitting the continuum, the line-to-continuum ratio does not depend on the sizes of the telescope beam used for the observations. Therefore, we can compute the D_2O OPR directly from the line-to-continuum ratios of the JCMT and *Herschel* observations, with no further correction. We note also that the para-D_2O line has an emission component that Butner et al. (2007) attributed to the hot corino region, whereas here we consider an *absorption* component only. In contrast, the ortho-D_2O line reported here exhibits absorption only because the emission component is probably diluted in the 35″ HIFI beam, which is much larger than the 15″ JCMT beam at 316 GHz.

Adopting the density and temperature profiles of the envelope of IRAS 16293 (Crimier et al. 2010), the gas at a distance larger (in radius) than 900 AU has a temperature lower than 30 K and a density lower than about 5×10^6 cm^{-3} (see Fig. 3). Thus, given the temperature of the gas absorbing the D_2O lines, we consider only the first two levels of each D_2O form. We use computed collisional rates for the two fundamental deexcitation transitions of ortho and para-D_2O with para-H_2 in the 10−30 K range of 2.3×10^{-11} and 3.8×10^{-11} cm^3 s^{-1} respectively (Wiesenfeld et al., in prep.). At the low temperatures found in the cold envelope, it is likely that H_2 is mainly in its para form (Pagani et al. 2009; Troscompt et al. 2009). For the collisional rates given above, the critical densities of the ortho- and para- D_2O fundamental transitions are 1×10^8 and 2×10^7 cm^{-3} respectively, and the upper levels of the two transitions are only moderately subthermally populated for a density of 5×10^6 cm^{-3}. For a two-level system, the species column density can be computed as

$$N_{tot} = \frac{8\pi v^3}{A_{ul}c^3} \Delta V \frac{\sqrt{\pi}}{2\sqrt{\ln 2}} \tau \frac{Q(T_{ex})}{g_u} \frac{\exp(E_u/kT_{ex})}{[\exp(h v/kT_{ex}) - 1]}, \quad (1)$$

where A_{ul} is the Einstein coefficient (2.96×10^{-3} s^{-1} for the ortho transition and 6.3×10^{-4} s^{-1} for the para transition), E_u is

Fig. 3. Density profile (solid line) and gas temperature profile (dot-dashed) of the IRAS 16293 envelope, as computed by Crimier et al. (2010). Values at a radial distance of about 900 AU are also indicated (see text). A distance of 120 pc was used in this computation (Loinard et al. 2008).

the upper level energy (E_u/k = 15.2 K for the para transition and =29.2 K for the ortho transition), g_u is the upper statistical weight ($3 \times (2J + 1)$ for the para transition, $6 \times (2J + 1)$ for the ortho transitions), v is the frequency (316.79981 GHz for the para transition and 607.349449 GHz for the ortho transition), ΔV is the linewidth (cm s^{-1}), and τ is the opacity at the line center. The parameter T_{ex} is the excitation temperature and $Q(T_{ex})$ its corresponding partition function. In the approximation of the escape probability formalism, T_{ex} is defined by the equation
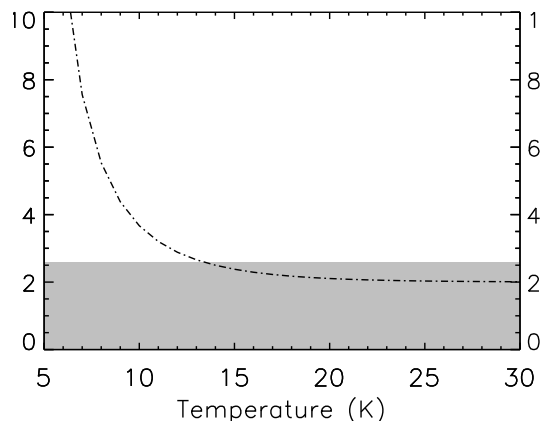
$$T_{ex} = \frac{h v/k}{h v/kT_k + \ln(1 + A_{ul}\beta/C_{ul})}, \quad (2)$$

where $C_{ul} = \gamma_{ul} \times n_{collision}$, $n_{collision}$ being the density of the collision partner (in this case para-H_2) and γ_{ul} being the collisional rate in cm^3 s^{-1} (values given above). The β parameter represents the probability that a photon at some position in the cloud escapes the system. For a static, spherically symmetric, and homogeneous medium, Osterbrock & Ferland (2006) derive this parameter as a function of the optical depth τ in the direction of the observer (see their Appendix 2). The opacity at the line center is expressed as a function of the line depth ($T_{abs} = T_C - T_L$) and the continuum (T_C)

$$\tau = -\ln\left(1 - \frac{T_{abs}}{T_C - J_v(T_{ex}) + J_v(T_{cmb})}\right), \quad (3)$$

where $J_v(T_{ex}) = (h v/k)/(\exp(h v/k) - 1)$ and T_{cmb} is the cosmic microwave background radiation temperature (2.73 K). In the limit of $\tau \gg 1$, $T_C - T_{abs} \sim J_v(T_{ex}) - J_v(T_{cmb})$, and $T_{ex} \sim 5$ K. Since the D_2O transitions are probably optically thin, we can reasonably assume that T_{ex} is lower than 5 K and $J_v(T_{ex}) - J_v(T_{cmb})$ is negligible.

As discussed above, we assume that the absorbing layer is much larger than the continuum emitting region. Owing to the uncertainty in the H_2 density (lower than 5×10^6 cm^{-3})

Fig. 4. Upper limit to the measured D_2O OPR (2.6, see text) as a grey box and the Boltzmann value (dotted-dashed line) as a function of temperature.

and the kinetic temperature (lower than 30 K), we applied the method described above to determine the column densities with $n_{H_2} = 10^6$ cm^{-3} and $T_{kin} \sim 20$ K. Table 1 lists the computation of the optical depths for both lines and their corresponding uncertainties. Since $\tau = -\ln(T_L/T_C)$, the uncertainty in the line optical depth is given by $\delta\tau = \exp(\tau) \times \delta(T_L/T_C)$. Our computation yields an OPR equal to 1.1 ± 0.4 with the corresponding column densities $N_{ortho} = (8.7 \pm 2.1) \times 10^{11}$ cm^{-2} and $N_{para} = (7.8 \pm 2.6) \times 10^{11}$ cm^{-2}. All errors here are 1σ. Both lines are optically thin and their T_{ex} are lower than 5 K. We note that decreasing the density and/or the kinetic temperature does not change the OPR by more than 10%. Therefore, the OPR is lower than 2.4 at a 3σ level of uncertainty (where we added the 3σ statistical error and the mentioned 10% to the 1.1 value). We assumed (see Sect. 2) that the relative gains to the lower and upper sidebands are equal. Since we do not have any information about the sideband ratio at the frequency of the D_2O line, we can only introduce a maximum uncertainty of 16%, corresponding to the overall calibration budget for band 1b. The resulting upper limit to the OPR is therefore increased to about 2.6. Figure 4 shows the measured OPR interval and the thermal equilibrium as a function of the gas temperature.

4. Conclusions

As discussed in Sect. 3, the gas absorbing the D_2O line is located more than 900 AU from the center and has a temperature that is lower than 30 K. The comparison between the upper value of the measured D_2O OPR and the thermal equilibrium value shows that they are consistent with a gas at a temperature of higher than about 15 K (at a 3σ level of confidence), and, therefore, with the assumed absorbing gas location. On the other hand, the D_2O gas may have formed in a previous phase, where the gas was colder, and, in this case, it means that it had the time to thermalise to the Boltzmann value. Unfortunately, given our poor knowledge of the mechanisms that can exchange the D_2O spins (see the Introduction), it is difficult here to infer the timescale for this change and, consequently, to provide a lower limit to the object age. On the other hand, the relatively large uncertainty in the OPR derived here does not allow either to exclude a non-thermal equilibrium situation. Higher signal-to-noise ratio observations will be needed to lower the uncertainty in the OPR value and derive a more robust result.

Using the density and temperature profiles of the envelope of IRAS 16293 by Crimier et al. (2010), the column density of the gas colder than 30 K is about 1×10^{23} cm^{-2}. Therefore, the D_2O abundance (with respect to H_2) is about 2×10^{-11}. An estimate of the water abundance profile will soon be available with the HIFI observations with a much higher spatial and spectral resolution than the one provided by the ISO observations (Ceccarelli et al. 2000). The D_2O molecules might form with one OPR, but then could freeze out on grain surfaces that could modify the ratio and then become desorbed. Owing to the high uncertainty in the H_2O abundance, we cannot at the time being completely exclude or confirm that formation can be described by grain surface chemistry. A modeling of the OPR evolution is beyond the scope of the present letter. With an improved calibration and better understanding of the instrumental effects, a more accurate determination of the D_2O OPR in this source and potentially other sources will be possible. ALMA may also hopefully yield an answer in the near future with the observation of cold D_2O with a higher spatial resolution.

To summarize, this Letter presents the first tentative estimate of the OPR for the D_2O molecule, demonstrating the outstanding capabilities of the HIFI instrument. The poor knowledge of the exchange mechanisms of the nuclear spins and the relatively large error in the derived OPR prevent us from drawing firm conclusions about the formation of heavy water at that time.

References

Bottinelli, S., Ceccarelli, C., Neri, R., et al. 2004, ApJ, 617, L69
Brünken, S., Müller, H. S. P., Endres, C., et al. 2007, Phys. Chem. Chem. Phys., 9, 2103
Butner, H. M., Charnley, S. B., Ceccarelli, C., et al. 2007, ApJ, 659, L137
Ceccarelli, C., Castets, A., Caux, E., et al. 2000, A&A, 355, 1129
Ceccarelli, C., Bacmann, A., Boogert, A., et al. 2010, A&A, 521, L22
Comito, C., & Schilke, P. 2002, A&A, 395, 357
Crimier, N., Ceccarelli, C., Maret, S., et al. 2010, A&A, 519, A65
de Graauw, Th., Phillips, T. G., Stutzki, J., et al. 2010, A&A, 518, L6
Emprechtinger, M., Lis, D. C., Bell, T., et al. 2010, A&A, 521, L28
Le Bourlot, J. 2000, A&A, 360, 656
Limbach, H., Buntkowsky, G., Matthes, J., et al. 2006, Chem. Phys. Chem., 360, 551
Lis, D. C., Phillips, T. G., Goldsmith, P. F., et al. 2010, A&A, 521, L26
Loinard, L., Torres, R. M., Mioduszewski, A. J., & Rodríguez, L. F. 2008, ApJ, 675, L29
Müller, H. S. P., Schlöder, F., Stutzki, J., & Winnewisser, G. 2005, J. Mol. Struct., 742, 215
Osterbrock, D. E., & Ferland, G. J. 2006, Astrophysics of gaseous nebulae and active galactic nuclei, ed. D. E. Osterbrock, & G. J. Ferland (CA: University Science Books)
Pagani, L., Vastel, C., Hugo, E., et al. 2009, A&A, 494, 623
Parise, B., Caux, E., Castets, A., et al. 2005, A&A, 431, 547
Pillbrat, G. L., Riedinger, J. R., Passvogel, T., et al. 2010, A&A, 518, L1
Rodgers, S. D., & Charnley, S. B. 2002, Planet. Space Sci., 50, 1125
Roelfsema, P. R., Helmich, F. P., Teyssier, D., et al. 2010, A&A, submitted
Troscompt, N., Faure, A., Maret, S., et al. 2009, A&A, 506, 1243

1 Centre d'Étude Spatiale des Rayonnements, Université Paul Sabatier, Toulouse, France
  e-mail: vastel@cesr.fr
2 CNRS/INSU, UMR 5187, Toulouse, France
3 Laboratoire d'Astrophysique de Grenoble, UMR 5571-CNRS, Université Joseph Fourier, Grenoble, France
4 Université de Bordeaux, Laboratoire d'Astrophysique de Bordeaux, Floirac, France
5 CNRS/INSU, UMR 5804, Floirac Cedex, France
6 Centro de Astrobiologìa, CSIC-INTA, Madrid, Spain
7 Laboratoire Interdisciplinaire Carnot de Bourgogne, UMR 5209-CNRS, Dijon Cedex, France
8 Department of Astronomy, University of Michigan, Ann Arbor, USA
9 California Institute of Technology, Pasadena, USA
10 Astronomical Institute Anton Pannekoek, University of Amsterdam, Amsterdam, The Netherlands
11 Department of Astrophysics/IMAPP, Radboud University Nijmegen, Nijmegen, The Netherlands
12 Laboratoire d'Études du Rayonnement et de la Matière en Astrophysique, UMR 8112 CNRS/INSU, OP, ENS, UPMC, UCP, Paris, France
13 Harvard-Smithsonian Center for Astrophysics, Cambridge MA, USA
14 Max-Planck-Institut für Radioastronomie, Bonn, Germany
15 Physikalisches Institut, Universität zu Köln, Köln, Germany
16 INAF - Istituto di Fisica dello Spazio Interplanetario, Roma, Italy
17 Infared Processing and Analysis Center, Caltech, Pasadena, USA
18 School of Physics and Astronomy, University of Leeds, Leeds, UK
19 INAF Osservatorio Astrofisico di Arcetri, Florence, Italy
20 IGN Observatorio Astronómico Nacional, Alcalá de Henares, Spain
21 Jet Propulsion Laboratory, Caltech, Pasadena, CA 91109, USA
22 SRON Netherlands Institute for Space Research, Groningen, The Netherlands
23 Max-Planck-Institut für Astronomie, Heidelberg, Germany
24 Ohio State University, Columbus, OH, USA
25 Johns Hopkins University, Baltimore MD, USA
26 INAF - Osservatorio Astronomico di Roma, Monte Porzio Catone, Italy
27 Institut de RadioAstronomie Millimétrique, Grenoble, France
28 Leiden Observatory, Leiden University, Leiden, The Netherlands
29 Kapteyn Astronomical Institute, University of Groningen, The Netherlands
30 Department of Physics and Astronomy, University College London, London, UK
31 Chalmers University of Technology, Gøterborg, Sweden